Univ.Roma I, 1078/94
cond-mat/9412069

Weighted Mean Field Theory for the Random Field Ising Model

David Lancaster[(a)], Enzo Marinari[(b)], Giorgio Parisi[(c)]

(a,c): Dipartimento di Fisica and INFN,
Università di Roma I *La Sapienza*,
Piazza A. Moro 2, 00185 Roma.

(b): Dipartimento di Fisica and INFN,
Università di Cagliari,
Via Ospedale 72, 09100 Cagliari.

Abstract: We consider the mean field theory of the Random Field Ising Model obtained by weighing the many solutions of the mean field equations with Boltzmann-like factors. These solutions are found numerically in three dimensions and we observe critical behavior arising from the weighted sum. The resulting exponents are calculated.

12/94

[(a)] (djl@liocorno.roma1.infn.it)
[(b)] (marinari@ca.infn.it)
[(c)] (parisi@roma1.infn.it)

1. Introduction

Despite progress since the early 1980's, when it was realised that perturbative techniques fail to capture its critical behavior, the Random Field Ising Model (RFIM)[1] is still in need of further illumination. The cause of the difficulty in dealing with this type of disorder is that the energy landscape is complicated, with many local minima that pertubation theory fails to take account of. Mean field theory provides a simple insight into the difficulty: at sufficiently low temperature the mean field equations have many solutions. The intuitively obvious way of defining mean field theory would be to weigh these solutions according to their Boltzmann factors. This weighted mean field theory, or to be precise, the theory with the weights $e^{-\beta F}$ which include an entropy factor, is the subject of this paper. In this context the failure of the pertubative approach comes about because, as is clear in the supersymmetric formulation[2], the prescription for the weights does not contain a Boltzmann factor.

In this report we solve the mean field equations numerically and directly construct the weighted mean field theory. Our main interest is to see how critical behavior can arise at the ferromagnetic transition. Guagnelli *et al.*[3] have analysed a truncation of the theory by only considering the maximal solutions: those with maximum or minimum magnetisation. They found that critical behavior does not arise in that case. Here we shall enlarge on their work by considering a much larger number of solutions and shall see how divergences in thermodynamic quantities can arise. The number of solutions included in the sum is clearly important in this approach and we shall discuss the issue in detail.

Replica theory is the natural setting for dealing with the difficulty mentioned above and although not yet successful in treating the critical behavior, it is helpful to keep the resulting scenario[4] in mind. The replica symmetric solution becomes unstable as one reduces the temperature below T_{RSB}, at which point the correlation length remains finite[5]. The critical temperature T_C at which ferromagnetic order arises is at a lower temperature $T_C < T_{RSB}$. Finally one expects replica symmetry to be restored at an even lower temperature. This scenario has clear analogues in our mean field treatment.

We start in sections 2 and 3 by discussing the consequences of weighted mean field theory and describing the technique of numerically searching for solutions. Section 4 is concerned with the general properties and number of solutions we find. Analysis of the correlation functions and the emergence of critical behavior is the subject of section 5. Finally we present a short conclusion discussing the numerical values of the exponents we determine.

2. The RFIM and its Weighted Mean Field Theory

The system consists of Ising spins subject to quenched random fields h_i;

$$H = -\sum_{\langle i,j \rangle} S_i S_j - \sum h_i S_i. \tag{2.1}$$

The effect of the fields is to destroy the tendency to long range order, and the original argument of Imry and Ma[6] based on the energy balance for domain formation gives the lower critical dimension as $d_{lcd} = 2$. Perturbative methods, which lead to the phenomenon of dimensional reduction[2,7], would instead predict $d_{lcd} = 3$. However in three dimensions it has been shown rigorously that long range order prevails at low enough temperature[8]. This case is most interesting and we shall restrict ourselves to studying the system in three dimensions.

In the work described here the fields are taken to be $\pm|h|$ with equal probability. According to arguments of Aharony[9], and consistent with the zero temperature simulations of Ogielski[10], a bimodal probability distribution of this sort causes the phase transition to be first order when $|h|$ is very large. As in [3] we work with $|h| = 1.5$, which is small enough to give a continuous transition, yet large enough to shift T_C substantially from its value without disorder, thus revealing a range of non-trivial critical behavior before the crossover to pure behavior at higher temperature.

For a given realisation of the random fields, the mean field equations for the system are:

$$m_i = \tanh\left(\beta(Dm_i + h_i)\right), \tag{2.2}$$

where m_i is the local magnetisation and Dm_i indicates a sum of the magnetisations over the nearest neighbours to site i. As has already been indicated, at low temperature there can be many solutions to this equation. We shall denote the solutions by m_i^α, and in general shall use the superscript α to denote a quantity, such as the free energy F^α, calculated for that solution.

$$F^\alpha = V\left(E^\alpha - \frac{1}{\beta}S^\alpha\right), \tag{2.3}$$

where the energy E^α, and entropy S^α, of the solution are given by the expressions,

$$\begin{aligned} E^\alpha &= -\frac{1}{V}\sum_i \frac{1}{2} m_i^\alpha D m_i^\alpha + h_i m_i^\alpha \\ S^\alpha &= -\frac{1}{V}\sum_i \frac{1+m_i^\alpha}{2}\log\left(\frac{1+m_i^\alpha}{2}\right) + \frac{1-m_i^\alpha}{2}\log\left(\frac{1-m_i^\alpha}{2}\right). \end{aligned} \tag{2.4}$$

A convenient way of organising the weighted mean field theory is in terms of a mean field partition function defined as:

$$Z_{MF} = \sum_{\alpha} e^{-\beta F^{\alpha}}. \tag{2.5}$$

This way of writing the theory simply encodes the intuitive definitions of quantities, such as the energy, as Boltzmann weighted sums over the solutions.

$$\frac{1}{V}\langle E\rangle = -\frac{1}{V}\frac{\partial \log Z_{MF}}{\partial \beta} = -\frac{1}{V}\sum_{\alpha}\frac{\partial}{\partial\beta}\left(\beta F^{\alpha}\right)\frac{e^{-\beta F^{\alpha}}}{Z_{MF}} = \sum_{\alpha} E^{\alpha}\frac{e^{-\beta F^{\alpha}}}{Z_{MF}} = \sum_{\alpha} w^{\alpha}E^{\alpha}, \tag{2.6}$$

where we have defined the weights: $w^{\alpha} = e^{-\beta F^{\alpha}}/Z_{MF}$. Note that $\partial F^{\alpha}/\partial\beta$ is simple only because of the constraints $\partial F^{\alpha}/\partial m_i^{\alpha} = 0$, which are nothing other than the mean field equations (2.2).

The average over the random fields is performed as the last step and is denoted by an overbar, for example $\overline{\langle E\rangle}$.

Critical behavior becomes apparent through study of the correlation functions. In the RFIM the correlators $\langle S_i S_j\rangle$ and $\langle S_i\rangle\langle S_j\rangle$ are both more singular in momentum space than the connected correlator $\langle S_i S_j\rangle_C = \langle S_i S_j\rangle - \langle S_i\rangle\langle S_j\rangle$. Although different from the field theory usage, it seems common in random field systems to call the correlator $\langle S_i\rangle\langle S_j\rangle$ "disconnected" and we shall follow this convention. In section 5 we shall determine the exponents $\bar{\eta}$ and η associated with the disconnected and connected correlators.

Contrary to ordinary mean field theory, the probability distribution implied by Z_{MF} is not factorised. The fluctuation dissipation theorem (FDT) is therefore not needed to calculate the correlation functions. Using Z_{MF} we find:

$$\langle S_i\rangle\langle S_j\rangle = (\sum_{\alpha} w^{\alpha}m_i^{\alpha})(\sum_{\gamma} w^{\gamma}m_j^{\gamma}) \tag{2.7}$$

$$\langle S_i S_j\rangle_C = (\sum_{\alpha} w^{\alpha}m_i^{\alpha}m_j^{\alpha}) - (\sum_{\alpha} w^{\alpha}m_i^{\alpha})(\sum_{\gamma} w^{\gamma}m_j^{\gamma}) + \frac{1}{\beta}\sum_{\alpha} w^{\alpha}g_{ij}^{\alpha}, \tag{2.8}$$

where g_{ij}^{α} is defined as $\partial m_i^{\alpha}/\partial h_j$ and is the usual term arising from the FDT.

3. Solving the Mean Field Equations

3.1. Iteration Technique

Starting from some seed configuration $m_i^{(0)}$, the mean field equations (2.2) are solved by iteration[11]:

$$m_i^{(t+1)} = \tanh\left(\beta(Dm_i^{(t)} + h_i)\right) . \tag{3.1}$$

This is implemented as an efficient code running on the APE parallel processor. We insist on strict convergence requirements, that for each solution $\sum_{board}(m_i^{(t+1)} - m_i^{(t)})^2 < 2.10^{-13}$. Where the m_i's are represented to float accuracy and there are 128 APE boards to cover the complete 32^3 lattice. With this requirement we find no difficulty in distinguishing solutions. The criterion for saying that two solutions are the same, that the maximal site difference $|m_i^\alpha - m_i^\gamma|$, be less than some cutoff, leads to the same identification of solutions for a wide range of cutoff values. We have finally chosen this cutoff to be 10^{-3}. Although the majority of seeds quickly converge, for some temperatures and some realisations of the random field we found that the convergence time was unacceptably large. A maximum number of 15000 iteration steps has been imposed, leading to rejection of about 1.4% of the potential solutions. We have observed a phenomenon known as "funneling" in which the configurations arising from different seeds rapidly converge to very similar configurations which then follow the same path though configuration space before finally converging[12]. The iteration technique may lead to solutions that are maxima of the free energy besides minima. Although we do not see such solutions in the cases described below, we have no simple way of rejecting them and they are implicitly included in the weighted sum.

3.2. Maximal Solutions

The iteration (3.1) has the property that if one can assign an ordering to two configurations m_a and m_b: $m_{a\ i}^{(t)} \geq m_{b\ i}^{(t)}$ for all sites i; then this ordering is preserved: $m_{a\ i}^{(t+1)} \geq m_{b\ i}^{(t+1)}$. Consequently one can identify two special, maximal solutions, m_+ and m_-, that arise from the seeds, $m_{+i}^{(0)} = 1$ and $m_{-i}^{(0)} = -1$, and that bound any other solution since $m_{+i}^{(t)} \geq m_{any\ seed\ i}^{(t)} \geq m_{-i}^{(t)}$. These were the solutions analysed in [3].

The existence of maximal solutions provides an accurate means of searching for the temperature (which by analogy with the replica analysis, we denote T_{RSB}) at which the mean field equations start to have more than one solution. Below this temperature m_+ and m_- differ. We have found T_{RSB} for series of random fields both on 32^3 and 64^3 lattices. At the larger size the peak of the distribution of T_{RSB}'s moves to higher temperature while the width shrinks – supporting the results from replica theory that T_{RSB} is well defined and separated from T_C in the thermodynamic limit. In about 10 percent of the cases we examined we observed two or more values of T_{RSB}. That is: at high temperature there is a unique solution, then as the temperature is reduced we first find more than one solution, then an interval where again only one solution exists, before finally reaching another low temperature region with many solutions. This effect is reminiscent of some of the observations of jumping made by Sourlas at zero temperature[13].

3.3. Seed Strategies

We have considered several strategies for the choice of seeds. The most efficient strategy we found was to consider chequerboard seeds: we divide the 32^3 cube up into 8 subcubes of size 16^3, and colour each one independently with $+1$ or -1. The leads to 256 seeds including the maximal ones. Further subdivision was thought to be impractical, so further sets of 256 seeds were generated by adding independent random pertubations to each site of the chequer seeds.

4. Number and Properties of Solutions

The number of solutions found and included in the weighted mean field theory is an important parameter. We start this section by displaying the average number and the effective number of solutions we find in our work. The main justification however, for curtailing the search for further solutions at the point we choose, is that the quantities measured from the correlators show very little change on increasing the number of solutions beyond those found with chequerboard seeds alone.

The results we shall present are based on data for the 32^3 periodic lattice for a set of 150 different magnetic field samples. We have calculated quantities based on the maximal solutions alone, and the solutions obtained from chequerboard seeds. Besides these, in the temperature region identified as most interesting, we have performed longer runs including chequerboard followed by two sets of chequerboard plus random seeds for the first 100 of the magnetic field samples. The temperature ranges covered by each of these three data sets are most clearly seen by looking ahead to the ranges of the three curves of fig. 2.

In all cases the temperature is measured in units of the mean field critical temperature for the pure model $T/T_{C\ pure} = T/6$.

Quantities such as the Energy, Entropy and Free Energy vary smoothly with temperature and the curves show little variation when the number of solutions included is increased. The average squared site magnetisation is also a smooth function, but the average magnetisation itself suffers large fluctuations. The specific heat starts to develop a cusp at the temperatures we shall later identify as the ferromagnetic phase transition.

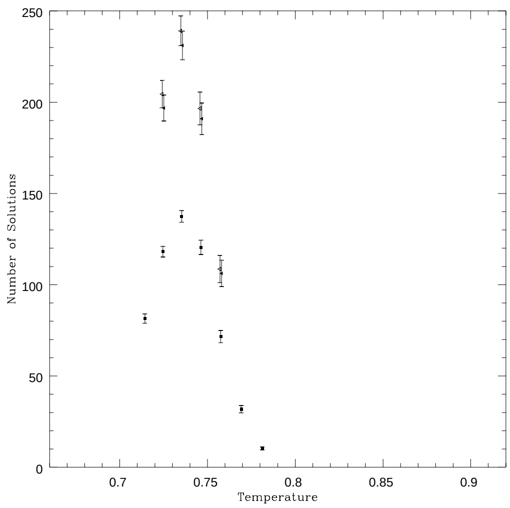

Fig. 1: Total number of solutions found. Squares for chequerboard seeds alone, triangles for chequerboard followed by one set of random pertubations added to chequerboard, open triangles for chequerboard followed by two such sets of random pertubations.

4.1. Number of solutions

The number of distinct solutions found by iteration is shown in fig. 1. Those solutions with completely negligible weight ($F^\alpha - F_{min} > 80$) have been dropped. The three sets of points are from successively increasing numbers of iteration trials. The lowest set (squares) is for the 256 chequerboard seeds while the upper two sets (triangles) correspond respectively to the addition of one and two sets of random pertubations on top of chequerboard.

Already from this figure it is clear that there is a law of diminishing returns relating the number of solutions found to the number of seeds iterated. From more detailed studies at a fixed low temperature, we see that after a steep initial rise, the number of solutions only increases slowly with the amount of effort. We have determined to stop searching for solutions at the point determined by the shoulder of this curve, which in practice is after the chequerboard and two sets of chequerboard plus random seeds. At higher temperatures a less though search is sufficient.

A feeling for the degree to which extra solutions are important comes from taking account of their weights, and a convenient quantity is W^2 defined by:

$$W^2 = \sum_\alpha (w^\alpha)^2. \tag{4.1}$$

The inverse gives the effective number of solutions that contribute. A plot of W^2 is shown in fig. 2 for maximal, chequerboard and chequerboard plus random seeds. At high temperatures $W^2 = 1$ since only one solution exists, whereas the rise at low temperatures is due to the increasing dominance of certain solutions. This increasing dominance can also be seen in the density of solutions in free energy which rises less steeply at lower temperatures. The fact that the effective number of solutions grows more slowly than the total number of solutions gives us our confidence that we are finding all the important solutions.

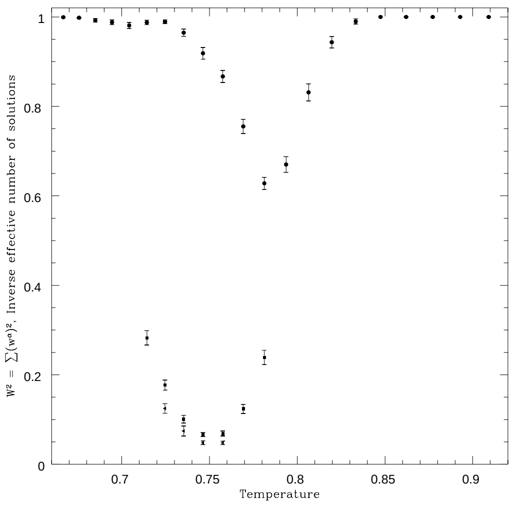

Fig. 2: $W^2 = \sum_\alpha (w^\alpha)^2$, the inverse of the effective number of solutions. Circles are for maximal solutions alone, squares for chequerboard, and triangles for chequerboard followed by (2 sets of) additional pertubations.

A histogram of the overlaps between different solutions displays a peak at small overlap with a long tail. When the histogram is normalised by the product of the weights of the solutions the peak moves to smaller overlap.

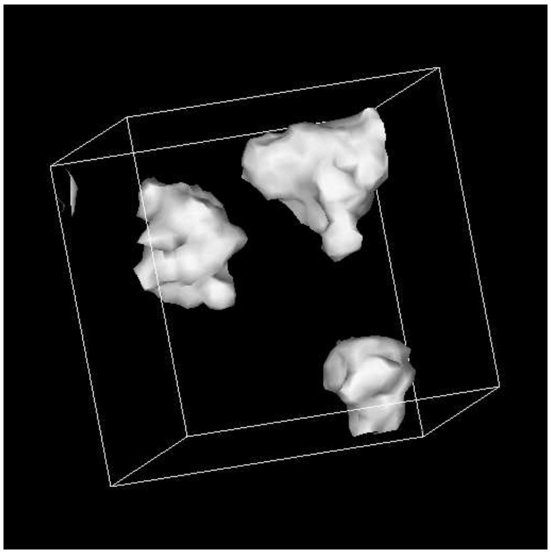

Fig. 3: Local differences between maximal solutions at temperatures just below T_{RSB}, isosurfaces of difference $m_{+i} - m_{-i} = 0.1$.

4.2. Form of solutions

There is a regime of temperature where it is possible to get some intuition into the form of the solutions. Generally the solutions are complicated: at high temperature m_i is small but follows the field $m_i \approx \beta h_i + \beta^2 D h_i$, whereas at low temperatures there is an overall magnetisation and sometimes reversed field domains. However, in the region just below T_{RSB} where there are only a small number of solutions, it is possible to see that the differences between solutions are local. In fig. 3a three dimensional picture of the difference in magnetisation between the maximal solutions (note that this is always positive) is shown by the constant difference surfaces. The dark region has small difference. The notable feature is that the regions of appreciable difference do not touch each other and are separated by a sea where the solutions are almost identical. This suggests that when the difference between maximal solutions has N local regions, each can be independently switched to either of two configurations, and that there should be a total of 2^N solutions. In fact, in the example corresponding to fig. 3, we do find a total of 8 solutions, and this method has been used to test the efficiency of different seed strategies. These solutions are found where the regions are local and do not influence each other. At such temperatures we must expect a constant density of such local differences between maximal solutions, and thus a total number of solutions that grows exponentially with the volume of the system. This picture fails at lower temperatures where the difference between maximal solutions is no longer local.

As was the case for the maximal solutions [3], in any particular solution correlation functions are rather rough with finite correlation length.

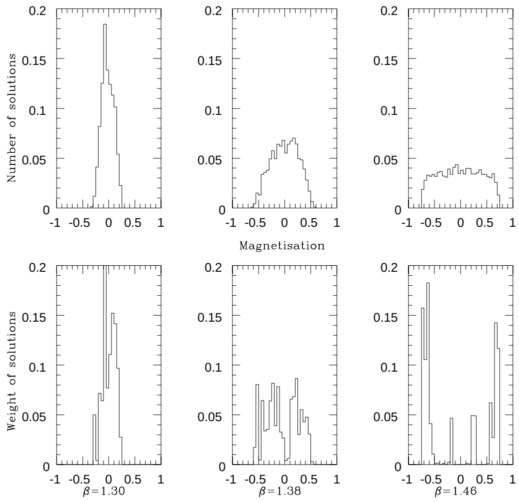

Fig. 4: Number (top line) and weight (bottom line) of solutions shown as a histogram against magnetisation for temperatures decreasing towards the right.

4.3. Below the transition

The reader will have noticed that our definition of mean field theory as a sum over *all* states is at variance with our usual understanding of the the ferromagnetic phase transition. One might try to modify the definition at low temperature by only including solutions with one sign of the magnetisation, however the region in the vicinity of the transition will remain unclear. It is possible to visualise how the transition takes place from the lists of solutions along with their magnetisations and weights. In the top row of fig. 4the number of solutions is shown as a histogram against their magnetisation. The width of the distribution increases at lower temperature, but there are always solutions of small magnetisation. In the lower line of plots in fig. 4 the summed weights rather than the number of solutions are shown. It is clear that at low temperature the small magnetisation solutions have low weight and are unimportant, and that the space of solutions is divided into two significant groups with opposite magnetisation.

5. Critical Behavior

In order to study critical behavior of the theory we look at the susceptibilities and the quantities that arise from analysing the correlation functions. Besides investigating the divergence of the correlation length, we expect two independent exponents defined by the behavior at the critical point. In three dimensional real space the disconnected case goes as $\sim r^{1-\bar{\eta}}$ whereas the connected case dies more quickly as $\sim r^{-1-\eta}$.

We always consider plane–plane correlators in one spatial direction with the transverse momenta set to zero: $G(x, k_y = 0, k_z = 0)$. From the solutions m_i^α two different lattice correlation functions, $C^{(1)}$ and $C^{(2)}$, can be defined using sums over transverse planes. For example in the x direction:

$$P_x^\alpha(x) = \frac{1}{L_y L_z} \sum_{y,z} m^\alpha(x, y, z). \tag{5.1}$$

For $C^{(1)}$, which is the plane–plane version of the disconnected correlator (2.7), the weighted sum over solutions is,

$$\begin{aligned} C_x^{(1)\alpha}(x) &= \frac{1}{L_x} \sum_{x_0} P_x^\alpha(x_0) P_x^\alpha(x_0 + x) \\ C_x^{(1)}(x) &= \sum_\alpha w^\alpha C_x^{(1)\alpha}(x). \end{aligned} \tag{5.2}$$

Instead of performing the sums in the order given above, we can first weight the plane sums before combining them,

$$\begin{aligned} P_x(x) &= \sum_\alpha w^\alpha P_x^\alpha(x) \\ C_x^{(2)}(x) &= \frac{1}{L_x} \sum_{x_0} P_x(x_0) P_x(x_0 + x). \end{aligned} \tag{5.3}$$

This procedure yields the plane–plane version $C^{(2)}$ of the first term in the connected correlator $\langle S_i S_j \rangle_C$, (2.8). An average over the principal directions and over the random fields is made before obtaining the final results for $\overline{C}^{(1)}$ and $\overline{C}^{(2)}$. The plane–plane connected correlator is given by $C^{(2)} - C^{(1)} + C^{(FDT)}$, in which the FDT term cannot be determined directly from the solutions m_i^α and a further iteration is required.

5.1. *Disconnected Correlator, $\langle S_i \rangle \langle S_j \rangle$*

Scaling arguments suggest that away from the critical point the 3 dimensional disconnected correlator behaves as $G(\mathbf{r}) = r^{1-\bar{\eta}} f(r/\xi)$. The scaling function we shall use to fit $C^{(1)}$ and define the correlation length arises from a Lorentzian squared propagator, a form that is motivated by zeroth order pertubation theory. This choice is recommended by its simplicity and it is frequently employed for fitting experimental data. The disadvantage of this choice of scaling function $f(r/\xi) = (\xi/r)^{1-\bar{\eta}} e^{-r/\xi}$, is that the critical limit, $\xi \to \infty$, amounts to $\bar{\eta} = 1$ behavior. Although $\bar{\eta}$ is in fact close to 1, we have explicitly checked that the other natural choice of scaling function $f(r/\xi) = e^{-r/\xi}$, gives similar results.

The plane–plane form of our fitting function is:

$$A\left(1+\frac{x}{\xi}\right)e^{-x/\xi}+B. \tag{5.4}$$

In contrast to the lack of sensitivity to the precise form of scaling function, it is important to make the periodic modification correctly. Since the correlations fall off so slowly, only keeping the leading two terms in the periodic sum leads to significant errors. We use the complete form:

$$\begin{aligned} &\frac{A}{(1-e^{-L/\xi})}\left(\left(1+\frac{x}{\xi}\right)e^{-x/\xi}+\left(1+\frac{L-x}{\xi}\right)e^{-(L-x)/\xi}\right) \\ &+\frac{Ae^{-L/\xi}}{(1-e^{-L/\xi})^2}\frac{L}{\xi}\left(e^{-x/\xi}+e^{-(L-x)/\xi}\right) \quad + \quad B. \end{aligned} \tag{5.5}$$

In all cases, even well away from the critical point, the fits are extremely good. Although we work exclusively above the critical temperature a constant term B has been included. This is done in order to take account of finite size effects and is also necessary to avoid discontinuities between data sets from different number of seeds. In the infinite system we would expect B to be the mean site magnetisation squared $\overline{\mathrm{m}}^2$; we however always observe it to be larger, approaching $\overline{\mathrm{m}^2}$ at low temperature. We shall regard B becoming different from zero as a signal of finite size effects being important.

In fig. 5 and fig. 6 the constant B and the correlation length obtained from the fitting are plotted against temperature. The jacknife technique is used for the errors, but note that they are correlated since the same set of random fields is used at each temperature. The plots are displayed for the maximal and for the chequerboard solutions. These sets of data flow smoothly into each other as do the points based on the solutions arising from chequerboard followed by chequerboard plus random seeds. In fact these later points lie well within the errors of the chequerboard points and are not shown. It is generally the case that extra solutions beyond chequerboard do not change any of our analysis of the disconnected correlator. For each of the fitting parameters the quantity $\overline{x^4}/3(\overline{x^2})^2$, remains close to 1 (its value for a gaussian distribution), except for the measurement of the constant term B at high temperatures where it becomes as large as 2.

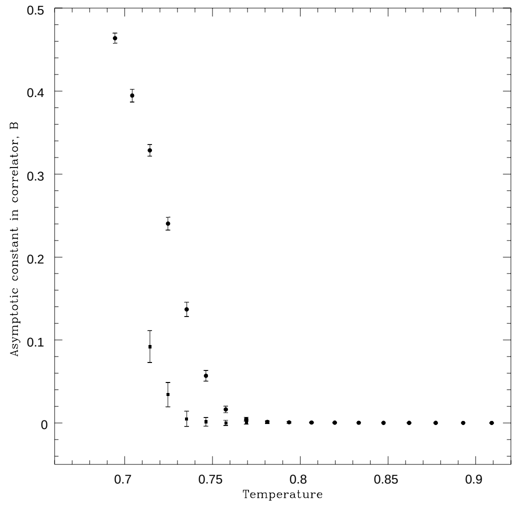

Fig. 5: Constant part of the disconnected correlator B, the squared magnetisation. Circles indicate results for maximal solutions alone, squares are for chequerboard solutions.

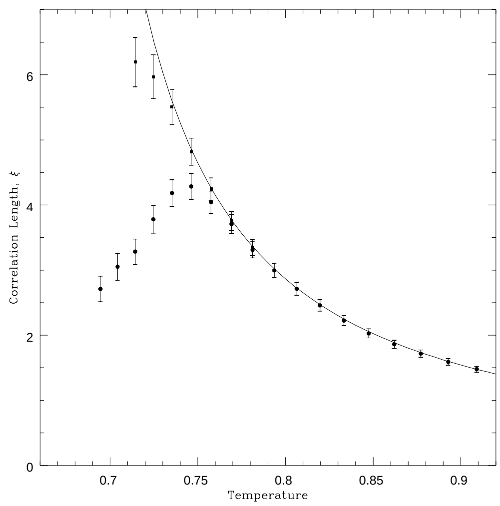

Fig. 6: Correlation Length ξ, from the disconnected correlator. Circles indicate results for maximal solutions alone, squares are for chequerboard solutions. The line shows the best fit, ignoring the lowest two points which are not consistent with $B = 0$.

Consider fig. 5 for the magnetisation squared as measured by the constant term B of the correlator. Significant deviations between the points calculated with many solutions and those calculated with only maximal solutions become apparent below the temperature at which the maximal solution B becomes non-zero ($T \sim 0.77$). The value of B calculated with many solutions remains zero to a lower temperature ($T \sim 0.74$) before it too becomes non zero, signalling either the onset of finite size effects or a breakdown of the approximation. In this temperature interval where deviations are clear yet the theory is reliable, the correlation length calculated from many solutions continues to grow while that of the maximal solutions rounds off. Certainly the rounded form coming from the maximal solutions is not a finite size effect as the curve for maximal solutions at 64^3 lies directly over this set. On the other hand the growing curve obtained from many solutions can become divergent as the size is increased since the number of solutions included will also increase. An exponent for this potential divergence can be determined by fitting the curve $\xi \sim (T - T_C)^{-\nu}$. To do this, a combination of points from different data sets that include as many solutions as available, is used. The two lowest temperature points where B is non-zero are dropped, while at the other end of the range the fit is found to be insensitive to the inclusion or not of high temperature points. We find ν to be 1.25 ± 0.11 where the errors are statistical from jacknife. The value of T_C found in this way is 0.64 ± 0.01.

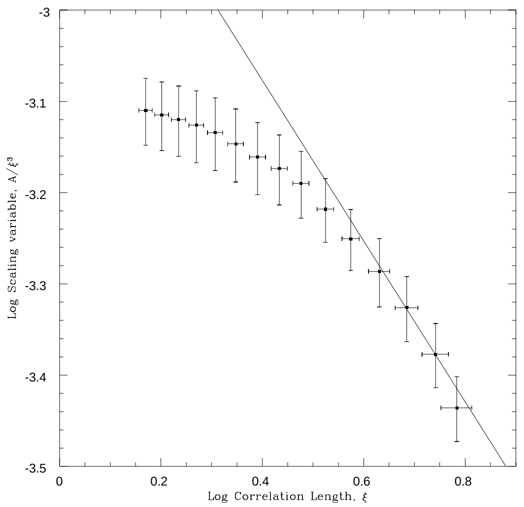

Fig. 7: The parameter A/ξ^3, from the disconnected correlator. Each point corresponds to the data set with most solutions available at that temperature. The last point is not included in the fit as $B \neq 0$.

The fit to the correlator, specifically the coefficient A, allows an estimate of the exponent $\bar{\eta}$. Scaling requires that the correlators $G(x, k_y = 0, k_z = 0)$ behave as $\xi^{3-\bar{\eta}} \tilde{G}(x/\xi)$, leading in the case of the fitting function (5.4), to $A \sim \xi^{3-\bar{\eta}}$. To avoid the uncertainty in T_C we plot $\log(A/\xi^3)$ against $\log(\xi)$ in fig. 7. In contrast to the situation for the correlation length this logarithmic plot is curved and the high temperature points adversely affect the exponent. The line shown on the figure is obtained as the slope of the last points which are consistent with $B = 0$. This provides an estimate of $\bar{\eta} = 0.89$ with a statistical error of ± 0.10. The systematic error associated with this measurement is harder to evaluate, but from the tendency of the lowest temperature points that were omitted, it is surely in a direction that would increase $\bar{\eta}$.

An alternative method of evaluating $\bar{\eta}$ would be directly through the susceptibility:

$$\chi^{(1)} = \frac{\beta}{V} \sum_{i,j} \langle S_i \rangle \langle S_j \rangle = \beta V \langle m \rangle^2 = \beta V \left(\frac{1}{V} \sum_i w^\alpha m_i^\alpha \right)^2 . \tag{5.6}$$

After the average over disorder we find that the susceptibility is given in terms of the magnetisation fluctuations $\overline{\chi}^{(1)} = \beta V \overline{\mathrm{m}^2}$ yielding a curve similar to the one obtained from the correlator fit. This curve does not however allow a determination of the exponent because in the critical low temperature region, $\overline{\mathrm{m}^2}$ is contaminated with parts coming from non-zero magnetisation causing the slope to actually turn positive for the points not consistent with $B = 0$.

5.2. Connected Correlator,

The analysis of the connected correlator requires more delicacy. There are two reasons for this; firstly the extra FDT term and secondly a strong sample dependence on the random field. By evaluating the quantity $\overline{x^4}/3(\overline{x^2})^2$ for the fitting parameters, one can see that in contrast to the disconnected case, the distributions are distinctly non-gaussian. This observation is reinforced by an inspection of the susceptibilities for individual magnetic fields where one often observes points far removed from the mean.

The full connected correlator is given by $C^{(2)} - C^{(1)} + C^{(FDT)}$. The FDT part $C^{(FDT)}$, defined in terms of $g_{ij}^\alpha = \partial m_i^\alpha / \partial h_j$ according to the plane–plane version of (2.8), cannot be determined directly from the magnetisations. In fact a separate iteration is required to solve the equation for g_{ij}^α:

$$g_{ij} = \beta(1 - m_i^2)(D g_{ij} + \delta_{ij}). \tag{5.7}$$

It would be prohibitive to perform this iteration for each site j of the lattice. However for a small number of cases we have done the iteration for one site fixed and note a strong dependence on the chosen site. We find that g_{ij} is more singular in position space than the part $C^{(2)} - C^{(1)}$ arising from the magnetisation, and that asymptotically g_{ij} always goes to zero. This is consistent with our theoretical prejudice that a fit of the FDT part alone should be done with the function arising from a propagator with a single pole in momentum space. At higher temperatures the FDT piece is dominant in the connected correlator, at lower temperatures it can plausibly be neglected. In that case, an analysis of $C^{(2)} - C^{(1)}$ alone leads to a correlation length, at the lowest few temperature points, that is within the errors of the same quantity, fig. 6, calculated for the disconnected correlator.

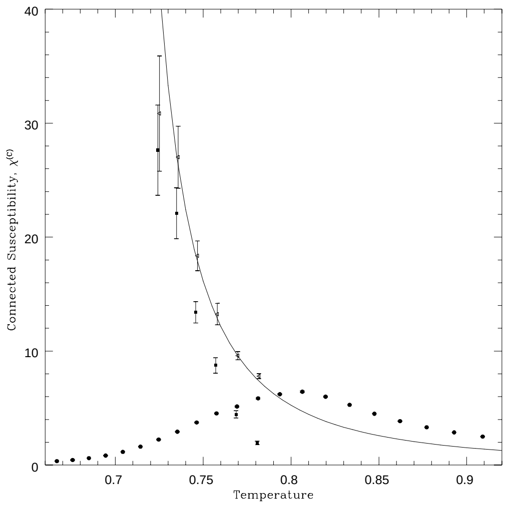

Fig. 8: Connected Susceptibility, $(\chi^{(2)} - \chi^{(1)})$ part shown with squares (chequerboard data), FDT piece $\chi^{(FDT)}$ shown with circles for the maximal solutions only (the errors are small), the sum $\chi^{(C)}$ shown with open triangles. The line shows the best fit using only low temperature points.

To determine the exponent η it is more convenient and accurate to abandon the full correlator and to work with the susceptibility.

$$
\begin{aligned}
\chi^{(C)} &= \frac{\beta}{V} \sum_{i,j} \langle S_i S_j \rangle_C = \chi^{(2)} - \chi^{(1)} + \chi^{(FDT)} \\
\chi^{(2)} - \chi^{(1)} &= \beta V \left((\sum_\alpha w^\alpha m^\alpha m^\alpha) - (\sum_\alpha w^\alpha m^\alpha)^2 \right) \\
\chi^{(FDT)} &= \frac{1}{V} \sum_{ij} \sum_\alpha w^\alpha g_{ij}^\alpha = \frac{1}{V} \sum_i \sum_\alpha w^\alpha g_i^\alpha .
\end{aligned}
\tag{5.8}
$$

The advantage of working with the susceptibility is that $g_i^\alpha = \sum_j g_{ij}^\alpha$ can be evaluated by a single iteration of the equation obtained by summing (5.7):

$$
g_i = \beta(1 - m_i^2)\,(D g_i + 1)\,. \tag{5.9}
$$

The term $\chi^{(FDT)}$ is not very sensitive to the number of solutions employed to calculate it. In fact, in the temperature region of interest the FDT term is small compared with the difference term and is well approximated by the contribution from the maximal solutions alone. On the other hand, the magnetisation difference term does show some dependence on the number of solutions; the dependence is still small, but leads to different estimates for the exponent. Both terms, $\chi^{(2)} - \chi^{(1)}$ and $\chi^{(FDT)}$, and their sum $\chi^{(C)}$ are shown in fig. 8. The crossover to pure behavior is very clear and using only the points below the crossover temperature we can attempt to determine the exponent η. The analog of the method used in the disconnected case, plotting $\chi^{(C)}/\xi^2$ against correlation length, fails because the curve turns and begins to rise at low temperature in the same way as for $\chi^{(1)}$ based on $\overline{m^2}$ We therefore resort to a direct determination of the susceptibility exponent γ defined by $\chi^{(C)} \sim (T - T_C)^{-\gamma}$. Because of the small number of points and the large errors the points are not weighted according to the size of their errors in this fit. We obtain $\gamma = 1.66 \pm 0.53$ with chequerboard data. For the increased number of solutions corresponding to chequerboard followed by two sets of random pertubations we find that γ is shifted to $\gamma = 1.97 \pm 0.91$, where the increased size of the error is due the reduced number of random fields in this sample. Using the scaling relation $\gamma = \nu(2 - \eta)$, we determine the exponent η to be $\eta = 0.7 \pm 0.5$ and $\eta = 0.4 \pm 0.8$ for these respective data sets.

6. Conclusion

By the direct procedure of solving the mean field equations for the RFIM we have analysed the natural mean field theory obtained by weighting the solutions with Boltzmann-like factors. Our main conclusion is that this theory can describe critical behavior at the ferromagnetic transition. The critical divergences arising from the sum over many solutions, each of which has regular behavior. We have investigated both the number and properties of the solutions that contribute.

The exponents we have determined are, $\nu = 1.25 \pm 0.11, \bar{\eta} = 0.89 \pm 0.10, \eta = 0.4 \pm 0.8$ where the errors are statistical. The most accurate determinations to date are from the work of Rieger and Young who use Monte Carlo and finite size scaling [14]. Our estimate of ν is consistent with their value of $\nu = 1.4 \pm 0.2$. Although our result for η lies close to their value of $\eta = 0.6 \pm 0.1$, our errors are so large that this hardly provides a stringent test of our method. Given the systematic errors involved in our determination of $\bar{\eta}$, which would tend to increase it, there is no contradiction with their value of $\bar{\eta} = 1.04 \pm 0.08$. As is clear from the decay of the disconnected correlator at criticality, $\bar{\eta}$ must be greater than 1 for consistency of this analysis. The fact that it is so close to 1 has led to suspicions of a first order transition [14],[15]. However we find it impossible to fit the specific heat, as measured by the derivative of the energy, to a divergence, and suspect a cusp form instead. There is thus the puzzle of zero latent heat already noted in [14]. In order to see how this effect in particular, and the analysis in general, depends on the choice of probability distribution for the random fields, we have been studying the gaussian distribution. Preliminary results suggest that conclusions are unaffected.

Only including those solutions that arise from chequerboard seeds gave good results for the disconnected correlator. Further accuracy would come from an increase in the number of random field samples rather than an increase in the number of solutions. In the connected case we observed stronger corrections coming from including solutions beyond chequerboard, however even there it was mainly the sample dependence that prevented greater accuracy.

Acknowledgments

D. L. would like to thank Remi Monasson for many helpful discussions.

References

[1] Nattermann T and Villain J, Phase Transitions **11** (1988) 5;
Belanger D P and Young A P, J. Magn. Magn. **100** (1991) 272.

[2] Parisi G and Sourlas N, Phys. Rev. Lett. **43** (1979) 744.

[3] Guagnelli M, Marinari E and Parisi G, J. Phys. **A26** (1993) 5675.

[4] Mézard M, Talk at the 16th Gwatt workshop on Magnetism, (1992)

[5] Mézard M and Monasson R, Phys. Rev. **B50** (1994) 7199.

[6] Imry Y and Ma S K, Phys. Rev. Lett. **37** (1975) 1399.

[7] Aharony A, Imry Y and Ma S K, Phys. Rev. Lett. **37** (1976) 1364;
Young A P, J. Phys. **C10** (1977) L275.

[8] Imbrie J Z, Phys. Rev. Lett. **53** (1984) 1747;
Imbrie J Z, Commun. Math. Phys. **98** (1985) 145.

[9] Aharony A, Phys. Rev. **B18** (1978) 3318.

[10] Ogielski A T, Phys. Rev. Lett. **57** (1986) 1251.

[11] Yoshizawa H and Belanger D P, Phys. Rev. **B30** (1984) 5220;
Ro C, Grest G S, Souloulis C M and Levin K, Phys. Rev. **B31** (1985) 1682.

[12] Mezard M, Private communication.

[13] Sourlas N, Talk at "Disordered Systems and Information Processing", Heraklion (1994)

[14] Rieger H and Young A P, J. Phys. **A26** (1993) 5279.

[15] Young A P and Nauenberg M, Phys. Rev. Lett. **54** (1985) 2429.